ELSEVIER

In vivo confocal imaging of the retina in animal models using scanning laser ophthalmoscopy

Mathias W. Seeliger [a,*], Susanne C. Beck [a], Naira Pereyra-Muñoz [a], Susann Dangel [b], Jen-Yue Tsai [d], Ulrich F.O. Luhmann [e], Serge A. van de Pavert [f], Jan Wijnholds [f], Marijana Samardzija [g], Andreas Wenzel [g], Eberhart Zrenner [c], Kristina Narfström [h], Edda Fahl [a], Naoyuki Tanimoto [a], Niyazi Acar [a,1], Felix Tonagel [a]

[a] Retinal Diagnostics Research Group, Tuebingen, Germany
[b] Molecular Genetics Laboratory, Tuebingen, Germany
[c] University Eye Hospital Dept. II, Tuebingen, Germany
[d] Biological Imaging Core, National Eye Institute, Bethesda, MD, USA
[e] Division of Medical Molecular Genetics and Gene Diagnostics, Institute of Medical Genetics, Zurich, Switzerland
[f] The Netherlands Ophthalmic Research Institute, Amsterdam, The Netherlands
[g] Laboratory for Retinal Cell Biology, University Hospital Zurich, Eye Clinic, Zurich, Switzerland
[h] Department of Medicine and Surgery, College of Veterinary Medicine, University of Missouri-Columbia, MO, USA

Abstract

Scanning-laser ophthalmoscopy is a technique for confocal imaging of the eye in vivo. The use of lasers of different wavelengths allows to obtain information about specific tissues and layers due to their reflection and transmission characteristics. In addition, fluorescent dyes excitable in the blue and infrared range offer a unique access to the vascular structures associated with each layer. In animal models, a further enhancement in specificity can be obtained by GFP expression under control of tissue-specific promotors. Important fields of application are studies in retinal degenerations and the follow-up of therapeutic intervention.
© 2005 Elsevier Ltd. All rights reserved.

Keywords: Scanning-laser ophthalmoscopy; Animal models; Retinal degenerations; Angiography

1. Introduction

Scanning-laser ophthalmoscopy (SLO) is a common diagnostic imaging technique in human ophthalmology. Although it does not provide colour images like a conventional fundus camera, the small beam width and the confocal diaphragm make it particularly attractive for the examination of small animal models. Laser light of shorter wavelengths (blue-green) is generally more strongly absorbed by ocular structures—especially melanin granules in the retinal pigment epithelium (RPE) and choroid—than that of longer ones (e.g., near infrared) (Preece & Claridge, 2002). Consequently, the short wavelength lasers provide higher contrast images of the retina but cannot penetrate the RPE/choroid in pigmented animals, whereas the infrared lasers give less retinal details but can 'see' through to the choroid and the sclera. The comparison of images taken with the different wavelengths provides information about specific tissues and layers due to their reflection and transmission characteristics. In addition, fluorescent dyes excitable in the blue and infrared range offer a unique access to the vascular structures associated with each layer.

The adaptation of SLO imaging for use in normal mouse models and those that carry specific genetic defects does provide valuable in vivo information about a number

---
* Corresponding author. Tel.: +49 7071 2980718; fax: +49 7071 294789.
  E-mail address: see@uni-tuebingen.de (M.W. Seeliger).
[1] Present address: Eye and Nutrition Research Group, National research on Agronomy, Dijon, France.

of ocular tissues from cornea through sclera. Here, we focus on vitreous, retina, RPE, and choroid, and the respective vascular elements. We also show the assessment of normally not visible structures feasible through GFP (green fluorescent protein) expression under control of tissue-specific promotors in transgenic animals. Another important field of application is the follow-up of therapeutic intervention in retinal degenerations and light damage. The non-invasive detection of expression markers like GFP in gene therapy and of structural improvements (an example of which we show here) does provide important information for the assessment of the therapeutic efficacy.

2. Methods

2.1. SLO imaging

For the work described here, we used a Heidelberg Engineering HRA I SLO (Heidelberg Engineering, Dossen-heim, Germany) modified for use with animals (Seeliger, Narfström, Reinhard, Zrenner, & Sutter, 2000). The HRA I features the two Argon wavelengths (488 nm and 514 nm) in the short wavelength range and two infrared diode lasers (795 nm and 830 nm) in the long wavelength range. The 488 and 795 nm lasers are used for fluorescein (FLA) and indocyanine green (ICG) angiography. Appropriate barrier filters of 500 and 800 nm, respectively, remove the reflected light with unchanged wavelength and allow only the light emitted by the dye upon stimulation to pass through (Fig. 1A).

Two device settings for the field of view were used throughout this paper, 20° for fundus overview, and 10° for detailed view, except in the cat model where a setting of 30° was used. As mentioned before, light of shorter wavelengths is generally more strongly diminished by ocular structures than that of longer ones; especially RPE and choroid are—in addition to the photoreceptors—the main absorbing tissues for visible light due to their melanin con-
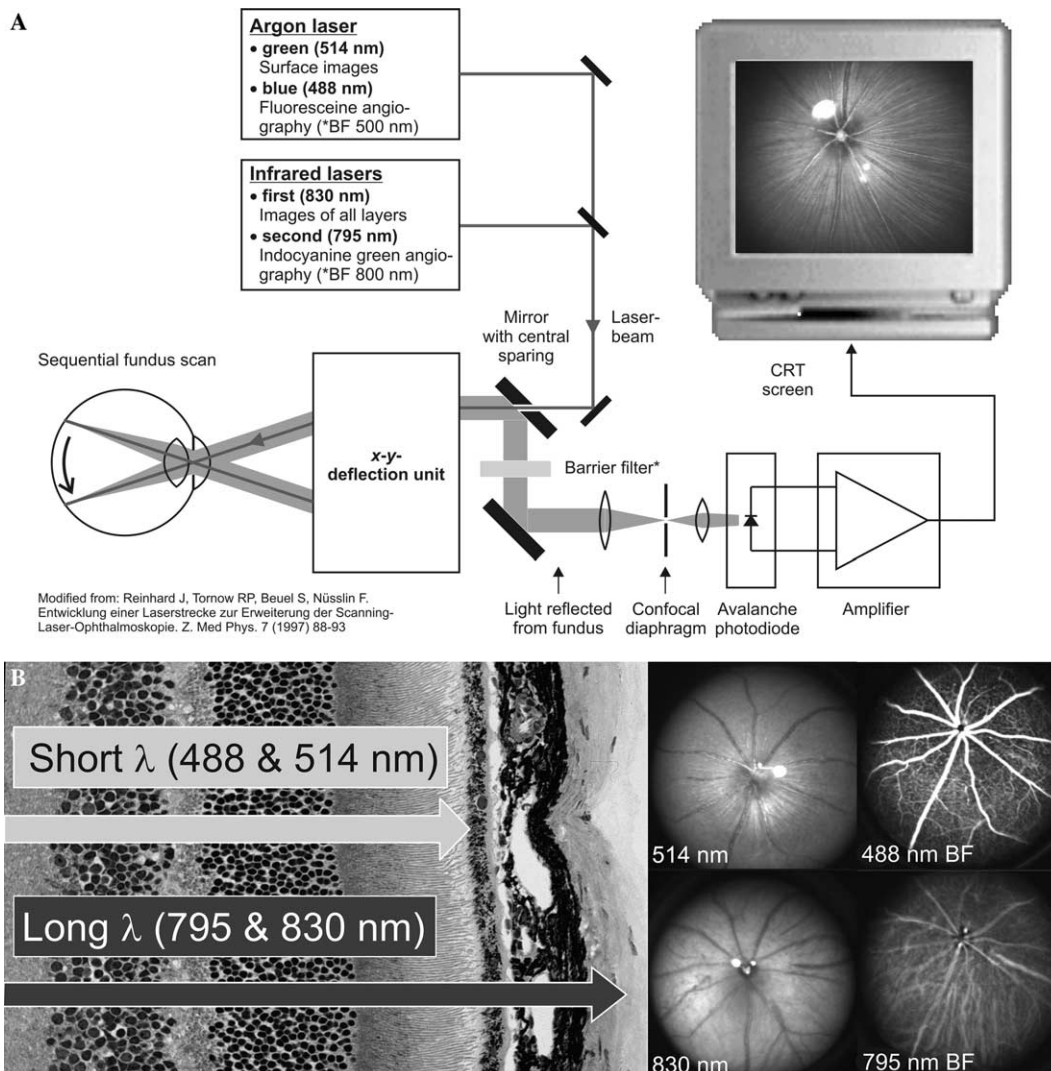

Fig. 1. Technical overview of scanning laser ophthalmoscopy (SLO). (A) Image generation in a confocal SLO system. (B) Layer selectivity of the different wavelengths. Short wavelength light cannot pass through the pigmented RPE/choroid, and the respective images show thus no subretinal structures.

tent. In pigmented animals, the short wavelength lasers provide the highest quality images of the retina, but cannot penetrate the RPE/choroid. In contrast, the infrared lasers show less retinal details but also reveal choroidal structures down to the sclera. Similarly, FLA provides the most detailed images of retinal capillaries, whereas ICG adds information about choroidal vessels but shows less details of retinal vasculature (Fig. 1B). An important difference between the dyes is their affinity to (large) plasma proteins. ICG is bound to such proteins more than 98%, whereas fluorescein is only bound to about 60–80% (Destro & Puliafito, 1989). As a consequence, ICG diffuses only very slowly out of the vascular lumen even if vessels are fenestrated, whereas fluorescein tends to leak rapidly (Destro & Puliafito, 1989).

2.2. Preparation of animals

Except for the dark adaptation, animals were prepared the same way as described for electroretinographic (ERG) recordings (Seeliger et al., 2001). In short, mice were anaesthetized by subcutaneous injection of ketamine (66.7 mg/kg) and xylazine (11.7 mg/kg), and their pupils dilated with tropicamide eye drops (Mydriaticum Stulln,

Pharma Stulln, Stulln, Germany). A custom-made contact lens was used to avoid dehydration of the cornea. FLA was performed using a s.c. injection of 75 mg/kg body weight fluorescein-Na (University pharmacy, University of Tuebingen, Germany), and ICGA following a s.c. injection of 50 mg/kg body weight ICG (ICG-Pulsion, Pulsion Medical Systems AG, Munich, Germany). All examinations were approved by a local ethics committee and were performed in accordance with the ARVO Statement for the Use of Animals in Ophthalmic and Vision Research.

3. Results

3.1. Imaging in normal retina

3.1.1. Native imaging

Native images obtained with the green (514 nm) and IR laser (830 nm) differ from each other (Fig. 2). The strong absorbance of green light by haemoglobin (Preece & Claridge, 2002) gives the thin-walled veins a dark appearance in the 514 nm images (Fig. 2A, black arrow; Fig. 2C). Branching points and capillaries that run for some distance parallel to the direction of the laser impose as dark spots (Fig. 2C, arrowhead) due to increased absorbance. Retinal
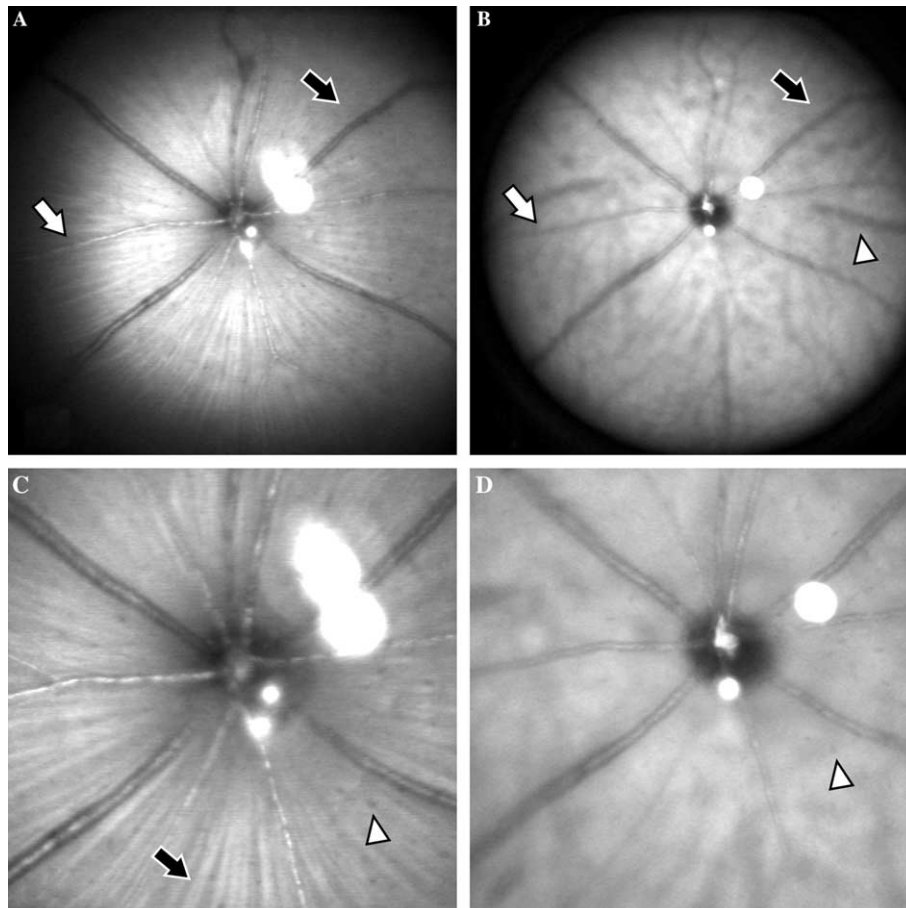

Fig. 2. Native SLO images obtained with green (514 nm; A and C) or infrared (830 nm; B and D) light in a normal mouse. (A and B) Fundus overview, (C and D) magnification of the retinal center. See text for further details.

arteries have a more silvery look, indicating that the light is reflected before it reaches the blood itself (Fig. 2A, white arrow; Fig. 2C). Although they have a strong muscular wall, they appear smaller than the veins, suggesting that the main site of reflection is close to the blood stream and not near the outside of the vessel (compare Fig. 4). In addition, the nerve fiber layer is usually well visible (Figs. 2A and C, arrow).

The IR images show less retinal details but provide additional information about the choroidal vasculature (Fig. 2B, arrowhead). Veins and arteries do not differ much in appearance in IR images (Fig. 2D). Branching points and capillaries that run for some distance parallel to the direction of the laser are also visible as dark spots (Fig. 2D, arrowhead); the same is true for choroidal blood pools (not shown).

3.1.2. Angiography

Both dyes, fluorescein and ICG, are present in the retinal as well as the choroidal circulation. However, the strong absorbance of the blue 488 nm laser by melanin does not permit subretinal structures to be seen in pigmented eyes. This is particularly hindered by the fact that the light would have to pass RPE and choroid twice – first to reach the dye and second on its way back to the detector, although this time with a slightly longer wavelength. FLA imaging yields the best images of the retinal capillaries—almost like a corrosion cast in vivo (Figs. 3 A and B). Large arteries and veins are not different in shade, but can be distinguished by diameter and often shape (arteries tend

to be more curved than the rather linear veins). Above the origin of the retinal vessels at the optic disc, a small cell conglomerate –presumably a remnant of the regressed vitreous vasculature– is found in mice (May & Lutjen-Drecoll, 2002), which blocks the light path and thus imposes as a dark structure (Figs. 3A, B, black arrowhead).

As the infrared light is much less affected by the presence of melanin, the ICG images depict both retinal and choroidal structures. In this situation, the confocal properties of the SLO help to select the plane of interest, so that the desired layer can be visualized. The most obvious choroidal pattern is formed by the two large ciliary vessels at nine and three o'clock (Figs. 3D and E, arrow). However, the degree of choroidal visibility decreases with the amount of melanin; it is best in a non-pigmented background (Fig. 3E) and somewhat lower in a strongly pigmented one like C57BL/6 (Fig. 3D). Nevertheless, pigmented backgrounds have the advantage to allow a separation of retinal and choroidal systems by comparison of fluorescein and ICG angiography.

In this work, the focus is on mouse eyes. A similar separation of retinal and choroidal information is however also achievable in larger animal models like cats (Figs. 3C and F). Whereas, the FLA image is limited to retinal vessels (Fig. 3C), the ICG image nicely reveals additionally the choroidal veins and arteries (Fig. 3F).

3.1.3. Autofluorescence

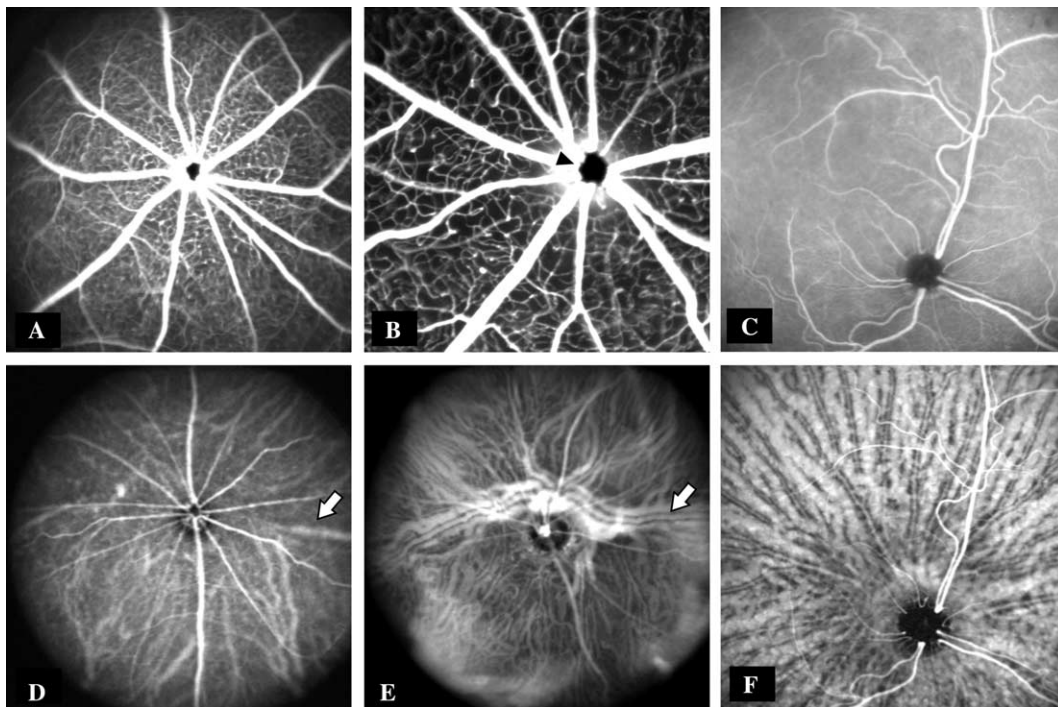Fundus autofluorescence (FAF) (Bellmann, Rubin, Kabanarou, Bird, & Fitzke, 2003) is a relatively new tech-

Fig. 3. SLO angiography following dye injection. (A–C) Fluorescence angiography (FLA) using fluorescein dye and a blue (488 nm) laser stimulus. (D–F) ICG angiography (ICGA) using indocyanine green dye and an infrared (795 nm) laser stimulus. (A and B) FLA in a normal mouse. (C) FLA in a cat. (D) ICGA in a C57BL/6 pigmented mouse. (E) ICGA in a BALB/c albino mouse. (F) ICGA in the same cat as in (C). See text for further details.

nique for the detection of fluorophores like lipofuscin in retinal and RPE cells (Delori et al., 1995).

The normal fundus in FAF features a diffuse "glow" of presumably normal lipids in retina and mainly RPE, which is blocked by the overlying vessels (Fig. 4A). Enhanced autofluorescence indicates a pathological accumulation of lipids (compare Fig. 6).

In mice, one can utilize the availability of transgenic models overexpressing the jellyfish green fluorescent protein (GFP) in different tissues. For example, if GFP is expressed under a cone opsin promotor (Fei & Hughes, 2001), one can get an in vivo wholemount-like display of the cone photoreceptors, which would be invisible otherwise (Fig. 4B). If crossed with a disease model, such a transgenic line can also be used to study the loss of cones due to a degenerative disease in an individual animal over time. Similarly, vascular targets can be labelled with GFP. A transgenic producing GFP under control of a smooth muscle α-actin promotor (SMAP) (Tsai, Yamamoto, Fariss, Hickman, & Pagan-Mercado, 2002) for example allows nicely to visualize the retinal vessels without application of a dye (Figs. 4C and D). The degree of visibility depends on the thickness of the muscular wall; arteries (A) are strongly labelled whereas veins (V) are hardly recognizable (Tonagel, Tanimoto, Fahl, Tsai, & Seeliger, 2005). Even single smooth muscle cells and pericytes in the vascular walls can be recognized, particularly in the smaller branches (Fig. 4D). The comparison of the native 514 nm image (Fig. 4C) and the FAF image (Fig. 4D) reveals that the muscular wall of the arterial system appears not to reflect the light, as the size of the arteries in the 514 nm image is much smaller than in the FAF image. In fact, the true outside diameter of both types seems to be rather similar (Fig. 4D).

3.2. Imaging in pathological conditions

3.2.1. Vascular developmental disorder

Norrie disease (Luhmann et al., 2005; Ohlmann et al., 2005) is an example of a condition where disease-related changes influence the maturation of ocular tissues. The main pathology is related to the inability of the retinal vascular system to produce the capillary network in the inner retina (Luhmann et al., 2005). As only surface vessels can
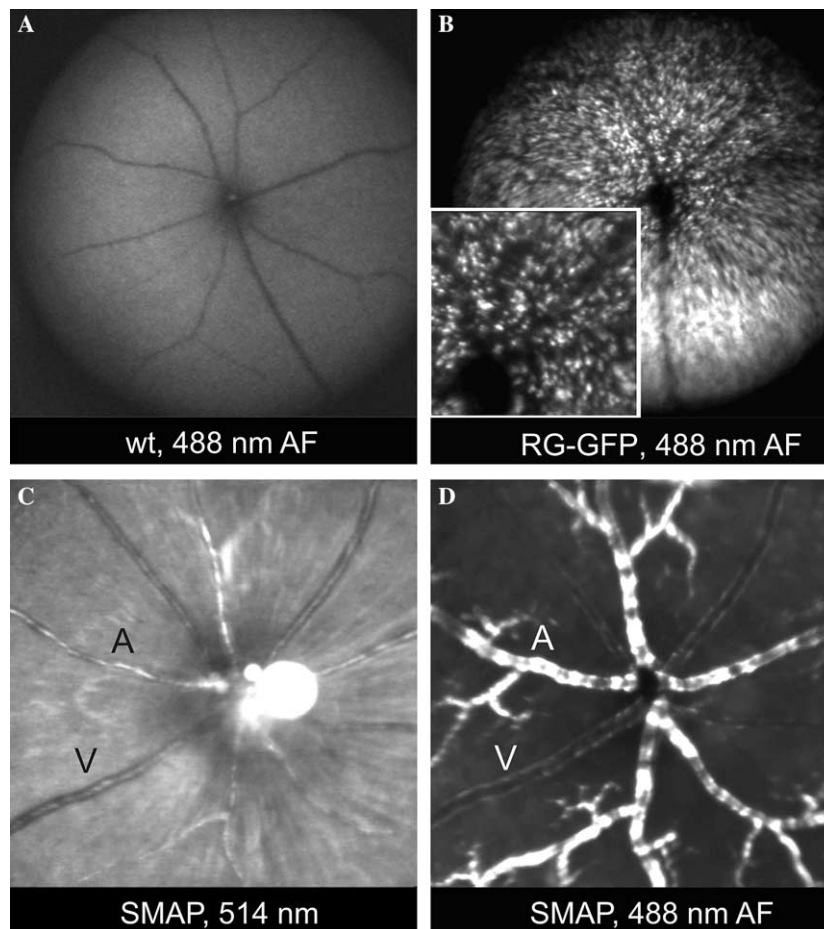

Fig. 4. Autofluorescence in normal and transgenic mice with tissue-specific GFP expression. (A) Fundus autofluorescence in a normal mouse. (B) Wholemount-like view of cones in a model expressing GFP under control of a cone opsin promotor. (C) Retinal vasculature in a transgenic model expressing GFP under control of a smooth muscle α-actin promotor (SMAP). (D) Visualization of the vascular wall fluorescence in SMAP transgenic mice. See text for further details.

be formed (Fig. 5C), a hypoxia of the inner retina results, causing upregulation of VEGF (vascular endothelial growth factor) (Luhmann et al., 2005). A probable side effect of VEGF is the persistence of a large number of vitreal vessels at postnatal day 14 (P14) and later on, which should have regressed by that time completely. ICG angiography is best suited to visualize such changes, as the dye is not subject to leakage from immature and VEGF-stimulated vessels (Fig. 5A). Whereas the major retinal arteries and veins seem to initially develop rather normally, the superficial retinal capillaries do form a layer of swollen-looking vessels (Fig. 5B). Their pattern indicates that they were guided by astrocytes during early postnatal development (Gariano, 2003). Again, ICG angiography was best suited to reveal this phenotype for the reasons stated above.

3.2.2. Neovascularization

Neovascularizations of retina and choroid (Campochiaro & Hackett, 2003) are rather rare in the natural course of degenerative diseases in mice, particularly most hereditary ones, but can be induced interventionally. However, they seem to occur also in diseases where the layer structure is disturbed like in Crumbs 1 (Crb1) knockout mice (van de Pavert et al., 2004). The site of a localized lesion is shown in Figs. 5D–E. FLA indicates the lesion nicely (Fig. 5D, arrow). The detail (Fig. 5E) reveals that there appears to be some traction pulling surrounding capillaries towards the

site of the lesion. Especially in cases of vascular and RPE changes, SLO imaging allows rapid and thorough screening of mouse mutant eyes, and thus facilitates a subsequent histomorphological analysis if the orientation of the globe is marked upon enucleation. Without the previous SLO examination, it would have been much more difficult to spot the small lesion histologically (Fig. 5F).

3.2.3. RPE pathology

Diseases of the RPE or tissues that relate to it may alter its function and morphology. Typical signs of altered RPE function are increased lipid content (yielding enhanced FAF) and/or depigmentation. In the example shown here, a deficiency in the gene for RPE65, an important protein of the visual cycle for the regeneration of rhodopsin, leads to a metabolic block of this cycle in the RPE (Redmond et al., 1998; Seeliger et al., 2001; Saari, 2001). As a consequence, retinyl esters accumulate in the cells and form large lipid droplets (Fig. 6C). As lipids give a stronger autofluorescence signal than the surroundings, these droplets can be well visualized in FAF imaging (Fig. 6B), whereas the 514 nm image (Fig. 6A) does not reveal much in this regard.

3.2.4. Therapeutic intervention

In disorders where morphological abnormalities can be detected with the SLO, their reversal by therapeutic inter-
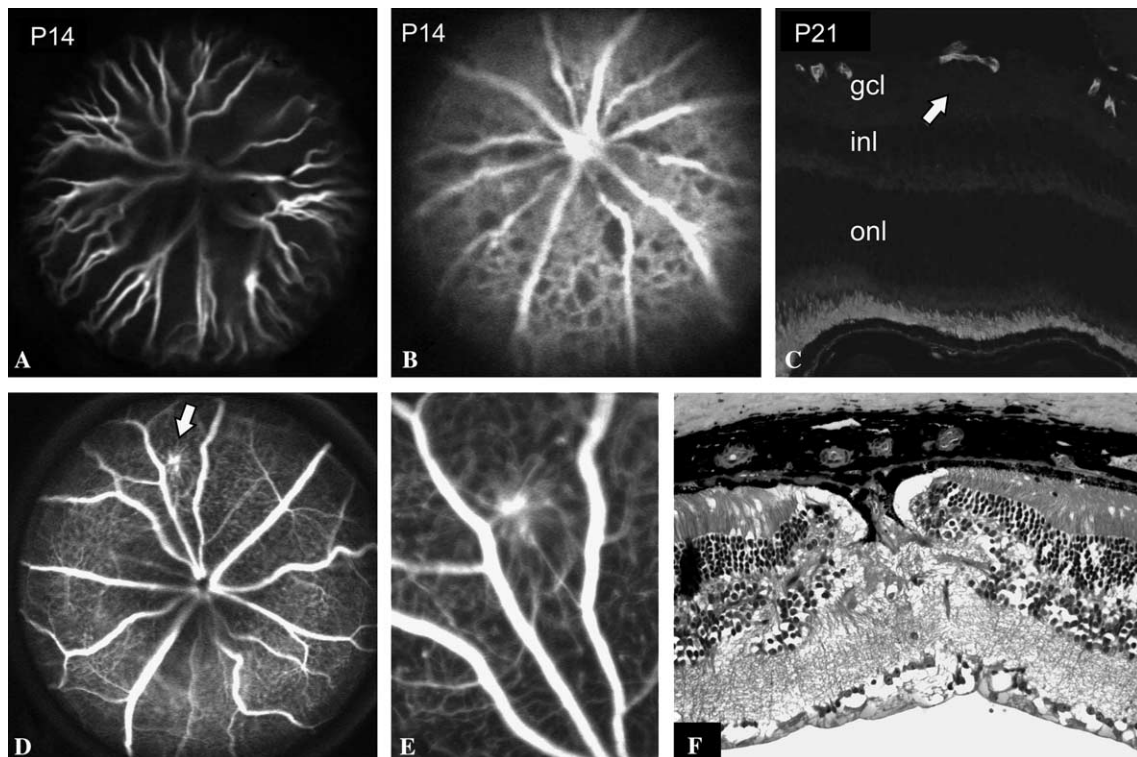

Fig. 5. Disease models I: Vascular development (A–C) and neovascularization (D–F). (A) Vitreous vessel persistence and (B) disturbance of regular capillary formation in Norrie disease mice (ICGA; modified from Luhmann et al., 2005). (C) Histological section showing the lack of inner retinal capillaries in Norrie disease mice (modified from Ohlmann et al., 2005). (D and E) Localized vascular abnormality in a Crumbs 1 (Crb1) knockout mouse (FLA) (F) Histological section of the respective site.
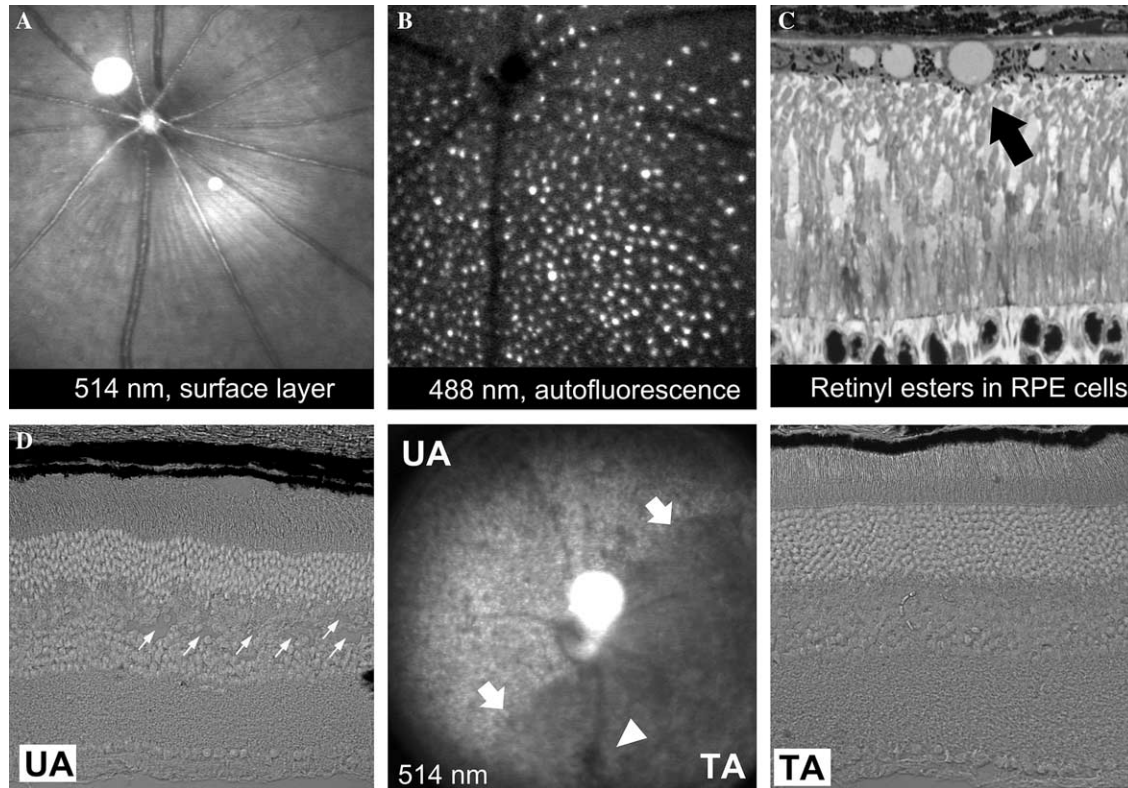
Fig. 6. Disease models II: RPE changes (A–C) and therapeutic intervention (D). (A) 514 nm surface and (B) autofluorescence image in RPE65-deficient mice. (C) Histological section showing the accumulation of lipid droplets in the RPE. (D) Comparison of treated (TA) and untreated areas (UA) in the fundus of RS1-deficient mice, the model for x-linked juvenile retinoschisis (modified from Min et al., 2005).

vention may be studied over time, too. In the present example, a model of X-linked juvenile retinoschisis (Weber et al., 2002) was treated with gene therapy based on an AAV system (Min et al., 2005). In the 514 nm image, the untreated area with the cyst-like lesions (Figs. 6D and UA) has a different appearance than the successfully treated regions (TA). The two arrows mark the border between UA and TA, and the arrowhead the site of injection.

4. Summary

This work highlights technical and diagnostic aspects of the use of scanning laser ophthalmoscopy in animal models for in vivo confocal imaging of the retina. The capabilities and limitations of the different imaging modes are discussed and examples for their application in normal and mutant animals are given. In particular, the ability to spot localized changes, which complements well the global functional in vivo tests like electroretinography, will certainly contribute to the spread of this technique in the future.

References

Preece, S. J., & Claridge, E. (2002). Monte Carlo modeling of the spectral reflectance of the human eye. *Physics in Medicine and Biology, 47*, 2863–2877.

Seeliger, M. W., Narfström, K., Reinhard, J., Zrenner, E., & Sutter, E. (2000). Continuous monitoring of the stimulated area in multifocal ERG. *Documents Ophthalmologica, 100*, 167–184.

Destro, M., & Puliafito, C. A. (1989). Indocyanine green videoangiography of choroidal neovascularization. *Ophthalmology, 96*, 846–853.

Seeliger, M. W., Grimm, C., Ståhlberg, F., Friedburg, C., Jaissle, G., Zrenner, E., Guo, H., Remé, Ch. E, Humphries, P., Hofmann, F., Biel, M., Fariss, R. N., Redmond, T. M., & Wenzel, A. (2001). New views on RPE65 deficiency: The rod system is the source of vision in a mouse model of Leber congenital amaurosis. *Nature Genetics, 29*, 70–74.

May, C. A., & Lutjen-Drecoll, E. (2002). Morphology of the murine optic nerve. *Investigative Ophthalmology & Visual Science, 43*, 2206–2212.

Bellmann, C., Rubin, G. S., Kabanarou, S. A., Bird, A. C., & Fitzke, F. W. (2003). Fundus autofluorescence imaging compared with different confocal scanning laser ophthalmoscopes. *The British Journal of Ophthalmology, 87*, 1381–1386.

Delori, F. C., Dorey, C. K., Staurenghi, G., Arend, O., Goger, D. G., & Weiter, J. J. (1995). In vivo fluorescence of the ocular fundus exhibits retinal pigment epithelium lipofuscin characteristics. *Investigative Ophthalmology & Visual Science, 36*, 718–729.

Fei, Y., & Hughes, T. E. (2001). Transgenic expression of the jellyfish green fluorescent protein in the cone photoreceptors of the mouse. *Visual Neuroscience, 18*, 615–623.

Tsai, J.-Y., Yamamoto, T., Fariss, R. N., Hickman, F. I., & Pagan-Mercado, G. (2002). Using SMAA-GFP mice to study pericyte coverage of retinal vessels. *Investigative Ophthalmology & Visual Science, 43*, E-Abstract 1929.

Tonagel, F., Tanimoto, N., Fahl, E., Tsai, J. Y., & Seeliger, M. W. (2005). In vivo study of retinal vasculature and function in SMAA–GFP mice. *Investigative Ophthalmology & Visual Science, 46*, E-Abstract 3164.

Luhmann, U. F., Lin, J., Acar, N., Lammel, S., Feil, S., Grimm, C., Seeliger, M. W., Hammes, H. P., & Berger, W. (2005). Role of the Norrie disease pseudoglioma gene in sprouting angiogenesis during development of the deep retinal vasculature. *Investigative Ophthalmology & Vision Science, 46*, 3372–3382.

Ohlmann, A., Scholz, M., Goldwich, A., Chauhan, B. K., Hudl, K., Ohlmann, A. V., Zrenner, E., Berger, W., Cvekl, A., Seeliger, M. W., & Tamm, E. R. (2005). Ectopic norrin induces growth of ocular capillaries and restores normal retinal angiogenesis in Norrie disease mutant mice. *Journal of Neuroscience, 25*, 1701–1710.

Gariano, R. F. (2003). Cellular mechanisms in retinal vascular development. *Progress in Retinal and Eye Research, 22*, 295–306.

Campochiaro, P. A., & Hackett, S. F. (2003). Ocular neovascularization: A valuable model system. *Oncogene, 22*, 6537–6548.

van de Pavert, S. A., Kantardzhieva, A., Malysheva, A., Meuleman, J., Versteeg, I., Levelt, C., Klooster, J., Geiger, S., Seeliger, M. W., Rashbass, P., Le Bivic, A., & Wijnholds, J. (2004). Crumbs homologue 1 is required for maintenance of photoreceptor cell polarization and adhesion during light exposure. *Journal of Cell Science, 117*, 4169–4177.

Redmond, T. M., Yu, S., Lee, E., Bok, D., Hamasaki, D., Chen, N., Goletz, P., Ma, J. X., Crouch, R. K., & Pfeifer, K. (1998). Rpe65 is necessary for production of 11-cis-vitamin A in the retinal visual cycle. *Nature Genetics, 20*, 344–351.

Saari, J. C. (2001). The sights along route 65. *Nature Genetics, 29*, 8–9.

Weber, B. H., Schrewe, H., Molday, L. L., Gehrig, A., White, K. L., Seeliger, M. W., Jaissle, G. B., Friedburg, C., Tamm, E., & Molday, R. S. (2002). Inactivation of the murine X-linked juvenile retinoschisis gene, Rs1h, suggests a role of retinoschisin in retinal cell layer organisation and synapse formation. *Proceedings of the National Academy of Sciences of the United States of America, 99*, 6222–6227.

Min, S. H., Molday, L. L., Seeliger, M. W., Dinulescu, A., Timmers, A. M., Janssen, A., Tonagel, F., Tanimoto, N., Weber, B. H., Molday, R. S., Hauswirth, W. W. (2005). Prolonged recovery of retinal structure and function after gene therapy in a Rs1h-deficient mouse model of human X-linked juvenile retinoschisis. *Molecular Therapy*, in press.